



# Constraints on the Helium Abundance from Fast Radio Bursts

Liang Jing and Jun-Qing Xia \*

Department of Astronomy, Beijing Normal University, Beijing 100875, China; 202021160013@mail.bnu.edu.cn

\* Correspondence: xiajq@bnu.edu.cn

**Abstract:** Through the relationship between dispersion measures (DM) and redshifts, fast radio bursts (FRBs) are considered to be very promising cosmological probes. In this paper, we attempted to use the DM- $z$  relationship of FRBs to study the helium abundance ( $Y_{\text{He}}$ ) in the universe. First, we used 17 current FRBs with known redshifts for our study. Due to their low redshifts and the strong degeneracy between  $Y_{\text{He}}$  and  $\Omega_b h^2$ , however, this catalog could not provide a good constraint on the helium abundance. Then, we simulated 500 low redshift FRB mock data with  $z \in [0, 1.5]$  to forecast the constraining ability on  $Y_{\text{He}}$ . In order to break the degeneracy between  $Y_{\text{He}}$  and  $\Omega_b h^2$  further, we introduced the shift parameters of the Planck measurement ( $R, l_A, \Omega_b h^2$ ) as a prior, where  $\Omega_b h^2$  represents the baryon density parameter, and  $R$  and  $l_A$  correspond to the scaled distance to recombination and the angular scale of the sound horizon at recombination, respectively. We obtained the standard deviation for the helium abundance:  $\sigma(Y_{\text{He}}) = 0.025$ . Finally, we considered 2000 higher redshift FRB data with the redshift distribution of  $[0, 3]$  and found that the constraining power for  $Y_{\text{He}}$  would be improved by more than 2 times,  $\sigma(Y_{\text{He}}) = 0.011$ , which indicates that the FRB data with high redshift can provide a better constraint on the helium abundance. Hopefully, large FRB samples with high redshift from the Square Kilometre Array can provide high-precision measurements of the helium abundance in the near future.

**Keywords:** cosmology; fast radio bursts; helium abundance; dispersion measure



Citation: Jing, L.; Xia, J.-Q.

Constraints on the Helium

Abundance from Fast Radio Bursts.

Universe 2022, 1, 0. <https://doi.org/>

Received: 18 April 2022

Accepted: 3 June 2022

Published:

**Publisher's Note:** MDPI stays neutral with regard to jurisdictional claims in published maps and institutional affiliations.



**Copyright:** © 2022 by the authors. Licensee MDPI, Basel, Switzerland. This article is an open access article distributed under the terms and conditions of the Creative Commons Attribution (CC BY) license (<https://creativecommons.org/licenses/by/4.0/>).

## 1. Introduction

Fast radio bursts (FRBs) are very short (ms) transients observed in frequencies from  $\sim 100$  MHz up to a few GHz [1–3]. The triggering mechanisms of FRBs are mysterious and still highly debated, but at least some FRBs can be produced by magnetar engines [4–7], also possibly by superconducting strings [8], or even by mysterious objects concerning strange quark stars [9]. The first FRB was discovered by Lorimer et al. [1], and hundreds of FRBs have been observed since then from several radio surveys, such as CHIME [10], Parkes [11], and ASKAP [12]. In the future, the Square Kilometre Array (SKA) is expected to detect  $\sim 10^4$  FRBs per decade [13]. Among those discovered FRBs, one repeating burst FRB121102 localized at  $z \sim 0.19$  established the cosmological origin of these events [14]. Furthermore, most FRBs have anomalously large dispersion measures (DM), which are related to their high redshifts. Through the relationship between DM and redshifts, FRBs are considered to be very promising cosmological probes. Several studies have been conducted to forecast the determinations of cosmological parameters using the future mock FRBs, such as the Hubble Constant [15,16], the dark energy equation of state [17], the fraction of baryon mass in the intergalactic medium (IGM) [18,19], the reconstruction of reionization using FRBs [20], and so on.

The helium abundance,  $Y_{\text{He}}$ , can be measured by the cosmic microwave background (CMB) since the damped tail of the CMB anisotropies is affected by the free electron density between the helium and hydrogen recombination, which is modified by variations in  $Y_{\text{He}}$  [21]. Using this method and allowing  $Y_{\text{He}}$  to vary as a derived parameter in the framework of

$\Lambda$ CDM model, Planck Collaboration et al. [22] gave the following constraints from the Planck TT, TE, EE, and lowE datasets at a 95% confidence level:

$$Y_{\text{He}} = 0.241 \pm 0.025. \quad (1)$$

In addition to the CMB anisotropies, the helium abundance can also affect the stellar evolution and galactic chemical evolution. Traditional measurements of the helium abundance are mainly based on the big bang nucleosynthesis (BBN) theory [23–25]. In this paper, we take the results of Aver et al. [23] as a reference, giving a slightly tighter constraint

$$Y_{\text{P}}^{\text{BBN}} = 0.2449 \pm 0.0040 (68\% \text{ CL}). \quad (2)$$

Several approaches also have been employed to constrain the helium abundance, by using the integrated spectra to infer the helium abundance of extragalactic globular clusters [26], via observations of metal poor HII regions to determine the primordial Helium abundance [27], by observations of the Extremely Metal-Poor Galaxies to determine the primordial helium abundance [28], and so on. However, these methods suffer from several uncontrolled systematic errors.

It is well known that the electron fraction,  $\chi_e$ , is directly related to the original hydrogen and helium abundances  $Y_{\text{H}}$  and  $Y_{\text{He}}$ . Using the electron fraction, we can see that there is a strong degeneracy between the DM of the FRB and  $Y_{\text{He}}$ . Therefore, if we can measure the DM of FRBs and establish a relationship between the DM and redshift and, in the meantime, use observations to precisely constrain other cosmological parameters, the helium abundance can also be measured by FRBs, avoiding large systematic errors. In this paper, we investigate the measurement of helium abundance using current and future FRB samples. We present methods for probing cosmological parameters via the DM- $z$  relationship in Section 2. In Section 3, we present the constraint results on  $Y_{\text{He}}$  from 17 current FRB samples. In Section 4, by introducing the shift parameters of the Planck measurements, we explore the possibilities of the helium abundance measurements by simulating future FRB samples. Finally, we present our conclusions in Section 5.

## 2. Properties of FRBs

The observed dispersion measure,  $\text{DM}_{\text{obs}}$ , is defined as the integral of the free electrons number density along the line of sight, which consists of the contributions from the IGM,  $\text{DM}_{\text{IGM}}$ ; the FRB host galaxy,  $\text{DM}_{\text{host}}$ ; and the Milky Way,  $\text{DM}_{\text{MW}}$  [2,29].  $\text{DM}_{\text{IGM}}$  from a fixed source redshift  $z$  is given by:

$$\text{DM}_{\text{IGM}}(z) = \int_0^z \frac{dz}{H(z)} \frac{n_e(z) f_{\text{IGM}}(z)}{(1+z)^2}, \quad (3)$$

where  $\Omega_b$  represents the baryon density parameter,  $E(z)$  is the dimensionless expansion function  $E(z) = H(z)/H_0$ , and  $f_{\text{IGM}}(z)$  represents the fraction of electrons in the IGM. Since we only consider the FRB sample with  $z < 3$  and assume that both hydrogen and helium are fully ionized, the cosmic electron density can be expressed as a function of the baryon abundance,  $n_e(z) = \rho_b(z) \chi_e(z) / m_p$ . Here,  $\rho_b(z)$  is the baryon mass density,  $m_p$  is the proton mass, and the electron fraction is:

$$\chi_e(z) = Y_{\text{H}} + \frac{1}{2} Y_{\text{He}} \approx (1 - Y_{\text{He}}) + \frac{1}{2} Y_{\text{He}} = 1 - \frac{1}{2} Y_{\text{He}}, \quad (4)$$

which is related to the primordial hydrogen and helium abundances. At present the CMB measurement provides the constraint on the helium abundance,  $Y_{\text{He}} = 0.241 \pm 0.025$  [22]. Since

there is little star formation at low redshifts, the overall fraction of electrons in the IGM does not evolve significantly over the redshift range covered by the FRB sample [18,19], and we simply keep  $f_{\text{IGM}} = 0.84$  constant.

Finally, we can write the relation between the DM and redshifts as:

$$\text{DM}_{\text{IGM}}(z) = \frac{3cH_0\Omega_b f_{\text{IGM}}}{8\pi G m_p} \left(1 - \frac{1}{2}Y_{\text{He}}\right) \int_0^z \frac{(1+z')dz'}{E(z')}, \quad (5)$$

where  $c$  represents the speed of light, and  $G$  is the gravitational constant.

The distribution of electrons in the IGM is inhomogeneous, and there is a stochastic contribution to the dispersion measure of a large scale structure, both of which lead to the complicated uncertainty of  $\text{DM}_{\text{IGM}}$ . In this paper, for simplicity, we consider a Gaussian distribution around the mean value of  $\text{DM}_{\text{IGM}}$ , and we interpolate the standard deviation linearly from the values found in simulations, using  $\sigma_{\text{IGM}}(z=0) \approx 40 \text{ pc cm}^{-3}$  and  $\sigma_{\text{IGM}}(z=1) \approx 180 \text{ pc cm}^{-3}$ . Due to the lack of understanding of the high redshift universe, we naively extend this relation,  $\sigma_{\text{IGM}}(z) \approx 40 + 140z \text{ pc cm}^{-3}$ , to the high redshift, which is roughly similar to the numerical simulation results [30] at  $z \sim 1.5$ . Since most of the FRB samples we have detected and the simulated samples that appear below lay at redshifts  $z < 2$ , the linear relationship we assume for  $\sigma_{\text{IGM}}$  affects the results very little.

For typical FRBs, there are two objects along the line of sight: the host halo and the Milky Way. The Milky Way DM can be predicted and removed with the help of models of the galactic electron distribution. We use the NE2001 model [31] to subtract the Milky Way contribution for each FRB position in the sky. For sources at high galactic latitude ( $|b| > 10^\circ$ ) where most FRBs are detected, the average uncertainty of the DM contribution from the Milky Way,  $\sigma_{\text{MW}}$ , is about  $30 \text{ pc cm}^{-3}$  [32]; therefore, we take  $\sigma_{\text{MW}} \approx 30 \text{ pc cm}^{-3}$  as a measure for the uncertainty of the model.

The host galaxy properties are more uncertain, due to the dependence on the type of the host galaxy, the relative orientations, and the near-source plasma, which are poorly known. Macquart et al. [33] estimated  $\text{DM}_{\text{host}} \approx 50/(1+z_{\text{host}}) \text{ pc cm}^{-3}$  theoretically from the localized FRBs. However, in our analysis, we further assume that the host halos are more or less similar to the Milky Way,  $\text{DM}_{\text{host}} \approx 100/(1+z_{\text{host}}) \text{ pc cm}^{-3}$ , conservatively, due to the large value of  $\text{DM}_{\text{host}} \in [55, 225] \text{ pc cm}^{-3}$  of FRB 121102, and allow for a large scatter  $\sigma_{\text{host}} \approx 50/(1+z_{\text{host}}) \text{ pc cm}^{-3}$  [29,34].

Of the hundreds of verified FRBs publicly available, only 19 FRBs have been localized at present, including the nearest repeating FRB 200110E [35] and FRB 181030A [36]. In our analysis, we mainly used the 17 localized FRBs<sup>1</sup>, which are listed in Table 1, to perform the numerical constraints and neglected the nearest FRB 200110E and FRB 181030A.

**Table 1.** Overview of all 17 FRBs with the measured redshift. The Milky Way DM is predicted by using the NE2001 model.

Name	Redshift	DM <sub>obs</sub> (pc cm <sup>−3</sup> )	DM <sub>MW</sub> (pc cm <sup>−3</sup> )	Telescope	Reference
FRB 121102	0.19273	557	188.0	Arecibo	Chatterjee et al. [37]
FRB 180916	0.0337	348.8	200.0	CHIME	Marcote et al. [38]
FRB 180924	0.3214	361.42	40.5	ASKAP	Bannister et al. [39]
FRB 181112	0.4755	589.27	102.0	ASKAP	Prochaska et al. [40]
FRB 190102	0.291	363.6	57.3	ASKAP	Bhandari et al. [41]
FRB 190523	0.66	760.8	37.0	DSA-10	Ravi et al. [42], Heintz et al. [43]
FRB 190608	0.1178	338.7	37.2	ASKAP	Chittidi et al. [44]
FRB 190611	0.378	321.4	57.8	ASKAP	Heintz et al. [43]
FRB 190614	0.6	959.2	83.5	VLA	Law et al. [45]
FRB 190711	0.522	593.1	56.4	ASKAP	Heintz et al. [43]
FRB 190714	0.2365	504.13	38.0	ASKAP	Heintz et al. [43])
FRB 191001	0.234	507.9	44.7	ASKAP	Heintz et al. [43]
FRB 200430	0.16	380.25	27.0	ASKAP	Heintz et al. [43]
FRB 201124	0.098	413.52	123.2	ASKAP	Day et al. [46], Ravi et al. [47]
FRB 180301	0.3304	536	152	Parkes	Bhandari et al. [48]
FRB 191228	0.2432	297.5	33	ASKAP	Bhandari et al. [48]
FRB 200906	0.3688	577.8	36	ASKAP	Bhandari et al. [48]

### 3. Constraints from Current Data

Assuming the flat  $\Lambda$ CDM model, in our calculations, we performed a global fitting analysis using the public CosmoMC software package [49], to constrain three parameters: the helium abundance  $Y_{\text{He}}$ , the Hubble constant  $H_0$ , and the dimensionless baryon density  $\Omega_b$ . Since we are studying the constraints on the helium abundance from FRBs, we set the choice of not using BBN consistency in our analysis, and our most general parameter space was:

$$\mathbf{P} \equiv (\Omega_b h^2, \Omega_c h^2, \Theta_s, \tau, Y_{\text{He}}, n_s, \ln(A_s)) \quad (6)$$

where  $\Omega_b$  and  $\Omega_c$  are the baryon and cold dark matter densities relative to the critical density,  $\Theta_s$  is the ratio (multiplied by 100) of the sound horizon at decoupling to the angular diameter distance to the last scattering surface,  $\tau$  is the optical depth to reionization,  $Y_{\text{He}}$  is the helium abundance, and  $A_s$  and  $n_s$  are the amplitude and the tilt of the power spectrum of the primordial scalar perturbations, respectively. Here, we set  $\Omega_c h^2 = 0.1202$ ,  $\tau = 0.0544$ ,  $n_s = 0.96$ , and  $\ln(A_s) = 3.1$  as fixed values and varied  $\Omega_b h^2$ ,  $\Theta_s$ , and  $Y_{\text{He}}$  in our analysis.

For the data analysis, we assumed Gaussian individual likelihoods to observe a dispersion measure  $\text{DM}_i$  at a given redshift  $z_i$ :

$$\mathcal{L}(\text{DM}_i, z_i) = \frac{1}{\sqrt{2\pi\sigma_i^2}} \exp\left(-\frac{(\text{DM}_i - \text{DM}_{\text{IGM}}(z_i))^2}{2\sigma_i^2}\right). \quad (7)$$

The total variance for the DM measurement of each FRB follows from the individual uncertainties accounting for the scatter of the IGM contribution, the MW electron distribution model, and the host galaxy:

$$\sigma_i^2(z_i) = \sigma_{\text{MW}}^2 + \sigma_{\text{host}}^2(z_i) + \sigma_{\text{IGM}}^2(z_i), \quad (8)$$

Apparently, at high redshifts, the uncertainty of  $\text{DM}_{\text{IGM}}$  will dominate the whole variance of the DM.

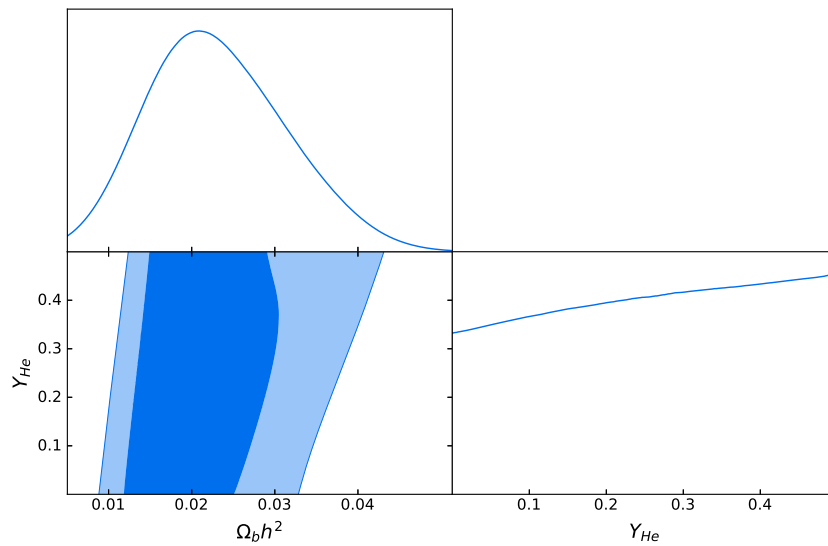


**Figure 1.** One-dimensional and two-dimensional constraints on the  $Y_{\text{He}}$  and  $\Omega_b h^2$  from the 17 current FRBs.

In Figure 1, we see that the current 17 FRB data had very limited constraining ability for the helium abundance, whose posterior distribution was almost flat. The main reason is that the redshifts of these 17 FRBs are relatively low, while the helium abundance is associated with the universe at higher redshifts. Therefore, it is impossible to understand cosmological information at high redshifts through these FRBs with low redshifts. Second, in Figure 1, we also show the constraint on the baryon energy density  $\Omega_b h^2$ , which was also very weak compared to other observations. According to Equation (5), there is a strong degeneracy between  $Y_{\text{He}}$  and  $\Omega_b h^2$ , which was also confirmed in the two-dimensional constraint of Figure 1. Therefore, it is very difficult to obtain useful results only from the 17 current FRBs' data.

#### 4. Future Prospects

The current limited FRB data can not provide precise constraints on the helium abundance. Fortunately, the amount of available FRBs is expected to grow quickly over the next few years. In this section, we investigate the constraining ability of FRBs on the helium abundance from a future mock sample.

##### 4.1. Mock Data

Qiang and Wei [50] studied the effect of the FRB redshift distribution on cosmological constraints in detail. However, the current limited samples can not provide us with the accurate information of FRBs' redshift distribution. For simplicity, we generated the mock data from the FRB redshift distribution following the galaxy distribution, which can be written as:

$$n(z) = z^2 \exp(-\alpha z), \quad (9)$$

where  $\alpha$  denotes the effective depth of the sample. Considering that the majority of FRB detection lies most likely at lower redshifts  $z < 1$ , we firstly created a sharp cutoff with  $\alpha = 7$  and, conservatively generated 500 samples up to  $z \sim 1.5$  (the conservative case). On the other hand, since the future SKA measurement has sufficient sensitivity to detect high-redshift FRBs, we also set  $\alpha = 3$  to generate 2000 samples up to  $z \sim 3$  for comparison (the high-redshift case). The fiducial values of the related parameters were:  $\Omega_b h^2 = 0.02230$ ,  $h = 0.671$ ,  $\Omega_m = 0.318$ ,

$Y_{\text{He}} = 0.24$ , and  $f_{\text{IGM}} = 0.84$  to generate  $\text{DM}_{\text{IGM}}$ , and the obtained sampling results are shown in Figure 2 for these two cases.

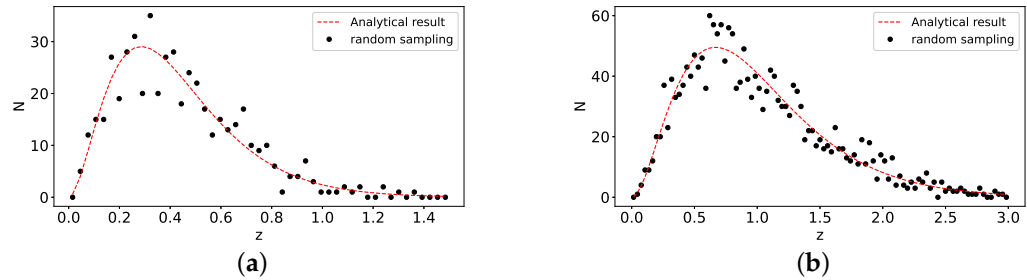


**Figure 2.** Redshift distributions of the simulated FRBs samples. (a) Conservative case: 500 FRBs with  $\alpha = 7$ . (b) High-redshift case: 2000 FRBs with  $\alpha = 3$ .

Extrapolating from the current uncertainty of the measurement, the constraint on the baryon energy density  $\Omega_b h^2$  was improved by a factor of 2, when considering the conservative case with  $N = 500$ . If we further consider the higher redshift case with  $N = 2000$  FRB data, the limit on  $\Omega_b h^2$  would further improved, and the standard deviation is about 0.002. However, as can be seen in Figure 3, unfortunately, no matter what kind of mock data we consider, it is still impossible to give a reasonably restricted result for the helium abundance. This is because although the number of mock data has enlarged, if we cannot provide better constraints on  $\Omega_b h^2$  by using other independent observations, the strong degeneracy between the helium abundance and the baryon energy density still cannot be broken, and the constraints on the helium abundance also will not be improved.

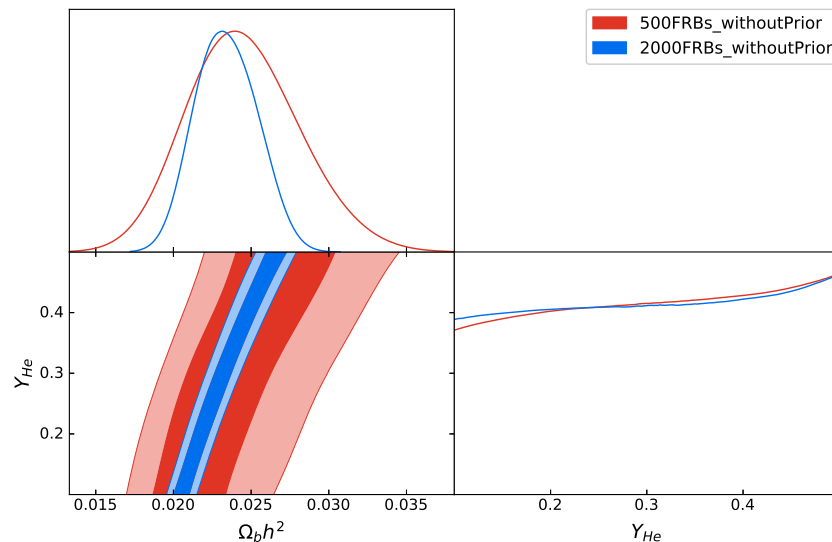


**Figure 3.** One-dimensional and two-dimensional constraints on the  $Y_{\text{He}}$  and  $\Omega_b h^2$  from the conservative case with  $N = 500$  (red) and the high-redshift case with  $N = 2000$  (blue).

#### 4.2. Shift Parameters

There are several studies on the degeneracies between cosmological parameters [51–53], and one way to break the degeneracy between  $Y_{\text{He}}$  and  $\Omega_b h^2$  is usually to use a Gaussian prior on  $\Omega_b h^2$ , as given by Cooke et al. [54]. In this paper, we introduce the shift parameters from the CMB measurements, which provides partial information of the CMB anisotropies, especially

the distance information, which can provide constraints of cosmological parameters to some extent without using the CMB full power spectra [55,56]. When compared with the CMB full data, we can obtain similar results on parameters by using the shift parameter method, without consuming too much time. In practice, we firstly used the full CMB power spectrum from Planck to obtain the best-fit values and the inverse covariance matrix of these shift parameters, and then input them into our calculations as a prior to break the degeneracy. It is worth noting that breaking the degeneracy with a Gaussian prior gives about the same effect; we introduced the method of shift parameters, since our calculations of the inverse covariance matrix among these shift parameters can also be applied in constraining other models.

The shift parameters,  $R$  and  $l_A$ , correspond to the scaled distance to recombination and the angular scale of the sound horizon at recombination, respectively, given by

$$R(z_*) = \sqrt{\Omega_m H_0^2} \chi(z_*) \quad (10)$$

$$l_A(z_*) = \pi \chi(z_*) / \chi_s(z_*) \quad (11)$$

where  $\chi(z_*)$  denotes the comoving distance to  $z_*$ , and  $\chi_s(z_*)$  denotes the comoving sound horizon at  $z_*$ . Furthermore, the decoupling epoch,  $z_*$ , is given by [57]

$$z_* = 1048 \left[ 1 + 0.00124 (\Omega_b h^2)^{-0.738} \right] \left[ 1 + g_1 (\Omega_m h^2)^{g_2} \right] \quad (12)$$

where

$$g_1 = \frac{0.0783 (\Omega_b h^2)^{-0.238}}{1 + 39.5 (\Omega_b h^2)^{0.763}}, \quad g_2 = \frac{0.560}{1 + 21.1 (\Omega_b h^2)^{1.81}}. \quad (13)$$

The comoving sound horizon  $\chi_s(z_*)$  is given by

$$\chi_s(z) = \frac{c}{\sqrt{3}} \int_0^{1/(1+z)} \frac{da}{a^2 H(a) \sqrt{1 + (3\Omega_b/4\Omega_\gamma)a}},$$

where  $\Omega_\gamma = 2.469 \times 10^{-5} h^{-2}$  for  $T_{\text{cmb}} = 2.725$  K, and

$$H(a) = H_0 \left[ \frac{\Omega_m}{a^3} + \frac{\Omega_r}{a^4} + \Omega_\Lambda \right]^{1/2}, \quad (14)$$

where  $\Omega_\Lambda$  is the dark energy density parameter, and the radiation density parameter,  $\Omega_r$ , is the sum of photons and relativistic neutrinos,

$$\Omega_r = \Omega_\gamma (1 + 0.2271 N_{\text{eff}}), \quad (15)$$

where  $N_{\text{eff}} = 3.04$  is the effective number of neutrino species.

We performed a global fitting analysis using the CosmoMC package to constrain  $R$ ,  $l_A$ , and  $\Omega_b h^2$  from the CMB power spectrum of the Planck measurement in the framework of the standard  $\Lambda$ CDM model. Our most general parameter space follows Equation (6), fixes  $Y_{\text{He}} = 0.24$ , and varies  $\Omega_b h^2$ ,  $\Omega_c h^2$ ,  $\Theta_s$ ,  $\tau$ ,  $n_s$ , and  $\ln(A_s)$  in our analysis. In Table 2, we list the mean values of  $R$ ,  $l_A$ , and  $\Omega_b h^2$  and the inverse covariance matrix among them. It is worth noting that the matrix we used was based on a fixed  $Y_{\text{He}} = 0.24$ , and the result did not change significantly if we vary  $Y_{\text{He}}$ .



Since we put the information of the shift parameters into the calculations, which is independent on the DM of the FRBs, the joint likelihood of the sample is then the product of the individual likelihoods, and the corresponding  $\chi^2$  function becomes:

$$\chi^2 = \chi_{\text{DM}}^2 + \chi_{\text{shift}}^2, \quad (16)$$

where the  $\chi^2$  function of shift parameters can be written as:

$$\chi_{\text{shift}}^2 = \left( x_i^{\text{th}} - x_i^{\text{data}} \right) \left( C_{ij}^{-1} \right) \left( x_j^{\text{th}} - x_j^{\text{data}} \right) \quad (17)$$

where  $x = (\Omega_b h^2, R, l_A)$  is the parameter vector, and  $(C_{ij}^{-1})$  is the inverse covariance matrix among these shift parameters, which is shown in Table 2. In our analysis, we adopted this updated likelihood function, which included the information of  $\Omega_b h^2$ , to break the degeneracy between  $Y_{\text{He}}$  and  $\Omega_b h^2$ .

**Table 2.** The mean values of shift parameters:  $l_A$ ,  $R$ , and  $\Omega_b h^2$  from the Planck measurement and the corresponding inverse covariance matrix among them.

	$l_A(z_*)$	$R(z_*)$	$\Omega_b h^2$
$l_A(z_*)$	$1.169 \times 10^2$	$-1.164 \times 10^3$	$5.325 \times 10^2$
$R(z_*)$	$-1.164 \times 10^3$	$9.236 \times 10^4$	$1.631 \times 10^6$
$\Omega_b h^2$	$5.325 \times 10^2$	$1.631 \times 10^6$	$7.844 \times 10^7$
Mean Value	$3.018 \times 10^2$	$1.750 \times 10^0$	$2.230 \times 10^{-2}$

#### 4.3. Results from DM and Shift Parameters

Firstly, we considered the conservative case with  $N = 500$  mock data. In Figure 4, we present the one-dimensional constraint on the helium abundance from the FRB DM data, together with the prior of shift parameters. We can clearly see that, due to the tight constraint on the baryon energy density,  $\sigma(\Omega_b h^2) = 0.0001$ , the degeneracy between  $Y_{\text{He}}$  and  $\Omega_b h^2$  has been broken entirely. The consequent constraint on the helium abundance becomes reasonable with the standard deviation  $\sigma(Y_{\text{He}}) = 0.025$ , instead of an almost flat distribution, as shown in Figure 3. Furthermore, this constraint is not much different from the current CMB constraint  $Y_{\text{He}} = 0.241 \pm 0.025$  at a 95% confidence level and BBN constraint  $\sigma(Y_{\text{P}}^{\text{BBN}}) = 0.004$ . This result indicates that with the help of external shift parameters information, we can use the DM of FRBs mock data to provide a good constraint on the helium abundance.



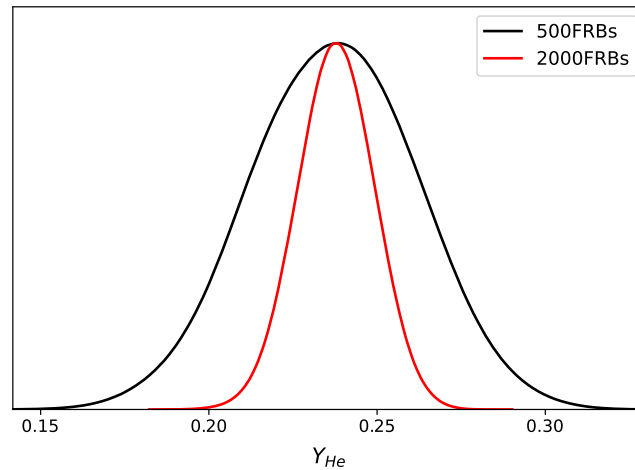


**Figure 4.** One-dimensional constraints on the helium abundance from the conservative case (black line) and the high-redshift case (red line), respectively.

Then, we moved to the high-redshift case with more FRB data  $N = 2000$  and a higher redshift distribution up to  $z \sim 3$ . Since the obtained error bar on the parameters should be smaller with  $N^{-1/2}$ , we expect that the constraint on the helium abundance would be improved by a factor of 2. In practice, we used the 2000 mock FRBs and the shift parameters to perform the analysis and obtain the standard deviation of the helium abundance  $\sigma(Y_{\text{He}}) = 0.011$ , which was slightly better than we expected, as shown in the red line of Figure 4. We think that this is due to the redshift distribution of these mock data, which was higher than the conservative case. We could have more information from the high redshift universe to study the helium abundance, which would be helpful to improve the constraint on  $Y_{\text{He}}$ . In the future, the SKA project expects to detect FRB samples with redshifts up to 14 [58], which implies FRB could be a very promising probe to study the high-redshift universe.

## 5. Conclusions

In this paper, we performed an analysis to study the helium abundance by using current and future FRB data, based on the DM- $z$  relation. Here, we summarize our main conclusions:

- Since the 17 current FRB samples have low redshift, resulting in poor quality of the samples, we could not obtain a useful constraint on the helium abundance, which is associated with the universe at higher redshifts.
- Then we simulated two mock data: the conservative case at low redshift and the high-redshift case. However, due to the strong degeneracy between the helium abundance and the baryon energy density, the constraints on  $Y_{\text{He}}$  were still very weak from the mock FRB data.
- Therefore, we introduced the distance information of shift parameters, derived from the CMB full power spectra of the Planck measurement. With this help, the constraint on the baryon energy density was significantly improved, and the degeneracy with  $Y_{\text{He}}$  was broken.
- Consequently, the constraints on the helium abundance were also improved with the standard deviation  $\sigma(Y_{\text{He}}) = 0.025$  and  $0.011$  for two FRBs' mock data, respectively. As can be seen from the current CMB constraint  $Y_{\text{He}} = 0.241 \pm 0.025$  at a 95% confidence level and BBN constraint  $\sigma(Y_{\text{p}}^{\text{BBN}}) = 0.004$ , the constraints from the FRBs are comparable. Hopefully, large FRB samples with high redshift from the Square Kilometre Array will provide high-precision measurements of the helium abundance in the near future.

**Author Contributions:** Formal analysis, J.-Q. X.; investigation, L.J.; Writing—original draft preparation, L.J.; Writing—review and editing, J.-Q.X. All authors have read and agreed to the published version of the manuscript.

**Funding:** J.-Q. Xia is supported by the National Science Foundation of China under grants No. U1931202 and 12021003; the National Key R&D Program of China No. 2020YFC2201603.

**Data Availability Statement:** Data relevant to this study are available on request to the corresponding author.

**Institutional Review Board Statement:** Not applicable

**Informed Consent Statement:** Not applicable

**Acknowledgments:** We thank Zheng-Xiang Li, Yang-Jie Yan, Ji-Ping Dai, and Ran Gao for useful discussions.

**Conflicts of Interest:** The authors declare no conflicts of interest.

## Notes

- <sup>1</sup> <http://frbhosts.org> (4th June,2022).

## References

1. Lorimer, D.R.; Bailes, M.; McLaughlin, M.A.; Narkevic, D.J.; Crawford, F. A Bright Millisecond Radio Burst of Extragalactic Origin. *Science* **2007**, *318*, 777, doi:10.1126/science.1147532.
2. Thornton, D.; Stappers, B.; Bailes, M.; Barsdell, B.; Bates, S.; Bhat, N.D.R.; Burgay, M.; Burke-Spolaor, S.; Champion, D.J.; Coster, P.; et al. A Population of Fast Radio Bursts at Cosmological Distances. *Science* **2013**, *341*, 53–56, doi:10.1126/science.1236789.
3. Petroff, E.; Bailes, M.; Barr, E.D.; Barsdell, B.R.; Bhat, N.D.R.; Bian, F.; Burke-Spolaor, S.; Caleb, M.; Champion, D.; Chandra, P.; et al. A real-time fast radio burst: Polarization detection and multiwavelength follow-up. *MNRAS* **2015**, *447*, 246–255, doi:10.1093/mnras/stu2419.
4. CHIME/FRB Collaboration.; Andersen, B.C.; Bandura, K.M.; Bhardwaj, M.; Bij, A.; Boyce, M.M.; Boyle, P.J.; Brar, C.; Cassanelli, T.; Chawla, P.; et al. A bright millisecond-duration radio burst from a Galactic magnetar. *Nature* **2020**, *587*, 54–58, doi:10.1038/s41586-020-2863-y.
5. Metzger, B.D.; Margalit, B.; Sironi, L. Fast radio bursts as synchrotron maser emission from decelerating relativistic blast waves. *MNRAS* **2019**, *485*, 4091–4106, doi:10.1093/mnras/stz700.
6. Kumar, P.; Bošnjak, Ž. FRB coherent emission from decay of Alfvén waves. *MNRAS* **2020**, *494*, 2385–2395, doi:10.1093/mnras/staa774.
7. Lu, W.; Kumar, P.; Zhang, B. A unified picture of Galactic and cosmological fast radio bursts. *MNRAS* **2020**, *498*, 1397–1405, doi:10.1093/mnras/staa2450.
8. Vachaspati, T. Cosmic Sparks from Superconducting Strings. *Phys. Rev. Lett.* **2008**, *101*, 141301, doi:10.1103/PhysRevLett.101.141301.
9. Geng, J.; Li, B.; Huang, Y. Repeating fast radio bursts from collapses of the crust of a strange star. *Innovation* **2021**, *2*, 100152, doi:10.1016/j.xinn.2021.100152.
10. CHIME/FRB Collaboration.; Amiri, M.; Bandura, K.; Berger, P.; Bhardwaj, M.; Boyce, M.M.; Boyle, P.J.; Brar, C.; Burhanpurkar, M.; Chawla, P.; et al. The CHIME Fast Radio Burst Project: System Overview. *ApJ* **2018**, *863*, 48, doi:10.3847/1538-4357/aad188.
11. Petroff, E.; Barr, E.D.; Jameson, A.; Keane, E.F.; Bailes, M.; Kramer, M.; Morello, V.; Tabbara, D.; van Straten, W. FRBCAT: The Fast Radio Burst Catalogue. *PASA* **2016**, *33*, e045, doi:10.1017/pasa.2016.35.
12. Johnston, K.; Oswalt, T.; Valls-Gabaud, D. Statistical Modeling and Analysis of Wide Binary Star Systems. In *Binary Stars as Critical Tools & Tests in Contemporary Astrophysics*; Hartkopf, W.I., Harmanec, P., Guinan, E.F., Eds.; Cambridge University Press: Cambridge, UK, 2007; Volume 240, p. 429.
13. Fialkov, A.; Loeb, A. A Fast Radio Burst Occurs Every Second throughout the Observable Universe. *Astrophys. J. Lett.* **2017**, *846*, L27, doi:10.3847/2041-8213/aa8905.
14. Spitler, L.G.; Scholz, P.; Hessels, J.W.T.; Bogdanov, S.; Brazier, A.; Camilo, F.; Chatterjee, S.; Cordes, J.M.; Crawford, F.; Deneva, J.; et al. A repeating fast radio burst. *Nature* **2016**, *531*, 202–205, doi:10.1038/nature17168.
15. Hagstotz, S.; Reischke, R.; Lilow, R. A new measurement of the Hubble constant using fast radio bursts. *MNRAS* **2022**, *511*, 662–667, doi:10.1093/mnras/stac077.
16. Wu, Q.; Zhang, G.Q.; Wang, F.Y. An 8 per cent determination of the hubble constant from localized fast radio bursts. *Mon. Not. R. Astron. Soc. Lett.* **2022**, slac022, doi:10.1093/mnrasl/slac022.
17. Gao, H.; Li, Z.; Zhang, B. Fast Radio Burst/Gamma-Ray Burst Cosmography. *ApJ* **2014**, *788*, 189, doi:10.1088/0004-637X/788/2/189.

18. Li, Z.; Gao, H.; Wei, J.J.; Yang, Y.P.; Zhang, B.; Zhu, Z.H. Cosmology-independent Estimate of the Fraction of Baryon Mass in the IGM from Fast Radio Burst Observations. *ApJ* **2019**, *876*, 146, doi:10.3847/1538-4357/ab18fe.
19. Dai, J.P.; Xia, J.Q. Reconstruction of baryon fraction in intergalactic medium through dispersion measurements of fast radio bursts. *Mon. Not. Roy. Astron. Soc.* **2021**, *503*, 4576–4580, doi:10.1093/mnras/stab785.
20. Dai, J.P.; Xia, J.Q. Reconstruction of reionization history through dispersion measurements of fast radio bursts. *J. Cosmol. Astropart. Phys.* **2021**, *2021*, 050, doi:10.1088/1475-7516/2021/05/050.
21. Planck Collaboration.; Ade, P.A.R.; Aghanim, N.; Arnaud, M.; Ashdown, M.; Aumont, J.; Baccigalupi, C.; Banday, A.J.; Barreiro, R.B.; Bartlett, J.G.; et al. Planck 2015 results. XIII. Cosmological parameters. *A&A* **2016**, *594*, A13, doi:10.1051/0004-6361/201525830.
22. Planck Collaboration.; Aghanim, N.; Akrami, Y.; Ashdown, M.; Aumont, J.; Baccigalupi, C.; Ballardini, M.; Banday, A.J.; Barreiro, R.B.; Bartolo, N.; et al. Planck 2018 results. VI. Cosmological parameters. *A&A* **2020**, *641*, A6, doi:10.1051/0004-6361/201833910.
23. Aver, E.; Olive, K.A.; Skillman, E.D. The effects of He I  $\lambda$ 10830 on helium abundance determinations. *J. Cosmol. Astropart. Phys.* **2015**, *2015*, 011, doi:10.1088/1475-7516/2015/07/011.
24. Peimbert, A.; Peimbert, M.; Luridiana, V. The primordial helium abundance and the number of neutrino families. *Rev. Mexicana Astron. Astrofis.* **2016**, *52*, 419,
25. Izotov, Y.I.; Thuan, T.X.; Guseva, N.G. A new determination of the primordial He abundance using the He I  $\lambda$ 10830 Å emission line: cosmological implications. *MNRAS* **2014**, *445*, 778–793, doi:10.1093/mnras/stu1771.
26. Leath, H.J.; Beasley, M.A.; Vazdekis, A.; Salvador-Rusiñol, N.; Gvozdenko, A. Inferring the helium abundance of extragalactic globular clusters using integrated spectra. *MNRAS* **2022**, *512*, 548–562. doi:10.1093/mnras/stac582.
27. Aver, E.; Olive, K.A.; Porter, R.L.; Skillman, E.D. The primordial helium abundance from updated emissivities. *J. Cosmol. Astropart. Phys.* **2013**, *2013*, 017, doi:10.1088/1475-7516/2013/11/017.
28. Matsumoto, A.; Ouchi, M.; Nakajima, K.; Kawasaki, M.; Murai, K.; Motohara, K.; Harikane, Y.; Ono, Y.; Kushibiki, K.; Koyama, S.; et al. EMPRESS. VIII. A New Determination of Primordial He Abundance with Extremely Metal-Poor Galaxies: A Suggestion of the Lepton Asymmetry and Implications for the Hubble Tension. *arXiv* **2022**, arXiv:2203.09617,
29. Deng, W.; Zhang, B. Cosmological Implications of Fast Radio Burst/Gamma-Ray Burst Associations. *ApJ* **2014**, *783*, L35, doi:10.1088/2041-8205/783/2/L35.
30. McQuinn, M. Locating the “Missing” Baryons with Extragalactic Dispersion Measure Estimates. *ApJ* **2014**, *780*, L33, doi:10.1088/2041-8205/780/2/L33.
31. Cordes, J.M.; Lazio, T.J.W. NE2001.I. A New Model for the Galactic Distribution of Free Electrons and its Fluctuations. *arXiv* **2002**, arXiv:astro-ph/0207156.
32. Manchester, R.N.; Hobbs, G.B.; Teoh, A.; Hobbs, M. The Australia Telescope National Facility Pulsar Catalogue. *AJ* **2005**, *129*, 1993–2006, doi:10.1086/428488.
33. Macquart, J.P.; Prochaska, J.X.; McQuinn, M.; Bannister, K.W.; Bhandari, S.; Day, C.K.; Deller, A.T.; Ekers, R.D.; James, C.W.; Marnoch, L.; et al. A census of baryons in the Universe from localized fast radio bursts. *Nature* **2020**, *581*, 391–395, doi:10.1038/s41586-020-2300-2.
34. Ioka, K. The Cosmic Dispersion Measure from Gamma-Ray Burst Afterglows: Probing the Reionization History and the Burst Environment. *ApJ* **2003**, *598*, L79–L82, doi:10.1086/380598.
35. Kirsten, F.; Marcote, B.; Nimmo, K.; Hessels, J.W.T.; Bhardwaj, M.; Tendulkar, S.P.; Keimpema, A.; Yang, J.; Snelders, M.P.; Scholz, P.; et al. A repeating fast radio burst source in a globular cluster. *Nature* **2022**, *602*, 585–589, doi:10.1038/s41586-021-04354-w.
36. Bhardwaj, M.; Kirichenko, A.Y.; Michilli, D.; Mayya, Y.D.; Kaspi, V.M.; Gaensler, B.M.; Rahman, M.; Tendulkar, S.P.; Fonseca, E.; Josephy, A.; et al. A Local Universe Host for the Repeating Fast Radio Burst FRB 20181030A. *ApJ* **2021**, *919*, L24, doi:10.3847/2041-8213/ac223b.
37. Chatterjee, S.; Law, C.J.; Wharton, R.S.; Burke-Spolaor, S.; Hessels, J.W.T.; Bower, G.C.; Cordes, J.M.; Tendulkar, S.P.; Bassa, C.G.; Demorest, P.; et al. A direct localization of a fast radio burst and its host. *Nature* **2017**, *541*, 58–61, doi:10.1038/nature20797.
38. Marcote, B.; Nimmo, K.; Hessels, J.W.T.; Tendulkar, S.P.; Bassa, C.G.; Paragi, Z.; Keimpema, A.; Bhardwaj, M.; Karuppusamy, R.; Kaspi, V.M.; et al. A repeating fast radio burst source localized to a nearby spiral galaxy. *Nature* **2020**, *577*, 190–194, doi:10.1038/s41586-019-1866-z.
39. Bannister, K.W.; Deller, A.T.; Phillips, C.; Macquart, J.P.; Prochaska, J.X.; Tejos, N.; Ryder, S.D.; Sadler, E.M.; Shannon, R.M.; Simha, S.; et al. A single fast radio burst localized to a massive galaxy at cosmological distance. *Science* **2019**, *365*, 565–570, doi:10.1126/science.aaw5903.
40. Prochaska, J.X.; Macquart, J.P.; McQuinn, M.; Simha, S.; Shannon, R.M.; Day, C.K.; Marnoch, L.; Ryder, S.; Deller, A.; Bannister, K.W.; et al. The low density and magnetization of a massive galaxy halo exposed by a fast radio burst. *Science* **2019**, *366*, 231–234, doi:10.1126/science.aay0073.
41. Bhandari, S.; Sadler, E.M.; Prochaska, J.X.; Simha, S.; Ryder, S.D.; Marnoch, L.; Bannister, K.W.; Macquart, J.P.; Flynn, C.; Shannon, R.M.; et al. The Host Galaxies and Progenitors of Fast Radio Bursts Localized with the Australian Square Kilometre Array Pathfinder. *ApJ* **2020**, *895*, L37, doi:10.3847/2041-8213/ab672e.

42. Ravi, V.; Catha, M.; D’Addario, L.; Djorgovski, S.G.; Hallinan, G.; Hobbs, R.; Kocz, J.; Kulkarni, S.R.; Shi, J.; Vedantham, H.K.; et al. A fast radio burst localized to a massive galaxy. *Nature* **2019**, *572*, 352–354, doi:10.1038/s41586-019-1389-7.
43. Heintz, K.E.; Prochaska, J.X.; Simha, S.; Platts, E.; Fong, W.f.; Tejos, N.; Ryder, S.D.; Aggerwal, K.; Bhandari, S.; Day, C.K.; et al. Host Galaxy Properties and Offset Distributions of Fast Radio Bursts: Implications for Their Progenitors. *ApJ* **2020**, *903*, 152, doi:10.3847/1538-4357/abb6fb.
44. Chittidi, J.S.; Simha, S.; Mannings, A.; Prochaska, J.X.; Ryder, S.D.; Rafelski, M.; Neeleman, M.; Macquart, J.P.; Tejos, N.; Jorgenson, R.A.; et al. Dissecting the Local Environment of FRB 190608 in the Spiral Arm of its Host Galaxy. *ApJ* **2021**, *922*, 173, doi:10.3847/1538-4357/ac2818.
45. Law, C.J.; Butler, B.J.; Prochaska, J.X.; Zackay, B.; Burke-Spolaor, S.; Mannings, A.; Tejos, N.; Josephy, A.; Andersen, B.; Chawla, P.; et al. A Distant Fast Radio Burst Associated with Its Host Galaxy by the Very Large Array. *ApJ* **2020**, *899*, 161, doi:10.3847/1538-4357/aba4ac.
46. Day, C.K.; Bhandari, S.; Deller, A.T.; Shannon, R.M.; Moss, V.A. ASKAP localisation of the FRB 20201124A source. *The Astronomer’s Telegram* **2021**, *14515*, 1.
47. Ravi, V.; Law, C.J.; Li, D.; Aggarwal, K.; Burke-Spolaor, S.; Connor, L.; Lazio, T.J.W.; Simard, D.; Somalwar, J.; Tendulkar, S.P. The host galaxy and persistent radio counterpart of FRB 20201124A. *arXiv* **2021**, arXiv:2106.09710.
48. Bhandari, S.; Heintz, K.E.; Aggarwal, K.; Marnoch, L.; Day, C.K.; Sydnor, J.; Burke-Spolaor, S.; Law, C.J.; Xavier Prochaska, J.; Tejos, N.; et al. Characterizing the Fast Radio Burst Host Galaxy Population and its Connection to Transients in the Local and Extragalactic Universe. *AJ* **2022**, *163*, 69, doi:10.3847/1538-3881/ac3aec.
49. Lewis, A.; Bridle, S. Cosmological parameters from CMB and other data: A Monte Carlo approach. *Phys. Rev. D* **2002**, *66*, 103511, doi:10.1103/PhysRevD.66.103511.
50. Qiang, D.C.; Wei, H. Effect of redshift distributions of fast radio bursts on cosmological constraints. *Phys. Rev. D* **2021**, *103*, 083536, doi:10.1103/PhysRevD.103.083536.
51. Scóccola, C.G.; Sánchez, A.G.; Rubiño-Martín, J.A.; Génova-Santos, R.; Rebolo, R.; Ross, A.J.; Percival, W.J.; Manera, M.; Bizyaev, D.; Brownstein, J.R.; et al. The clustering of galaxies in the SDSS-III Baryon Oscillation Spectroscopic Survey: constraints on the time variation of fundamental constants from the large-scale two-point correlation function. *MNRAS* **2013**, *434*, 1792–1807, doi:10.1093/mnras/stt1143.
52. Keisler, R.; Reichardt, C.L.; Aird, K.A.; Benson, B.A.; Bleem, L.E.; Carlstrom, J.E.; Chang, C.L.; Cho, H.M.; Crawford, T.M.; Crites, A.T.; et al. A Measurement of the Damping Tail of the Cosmic Microwave Background Power Spectrum with the South Pole Telescope. *ApJ* **2011**, *743*, 28, doi:10.1088/0004-637X/743/1/28.
53. Caramete, A.; Popa, L.A. Cosmological evidence for leptonic asymmetry after Planck. *J. Cosmol. Astropart. Phys.* **2014**, *2014*, 012, doi:10.1088/1475-7516/2014/02/012.
54. Cooke, R.J.; Pettini, M.; Steidel, C.C. One Percent Determination of the Primordial Deuterium Abundance. *ApJ* **2018**, *855*, 102, doi:10.3847/1538-4357/aaab53.
55. Wang, Y.; Mukherjee, P. Observational constraints on dark energy and cosmic curvature. *Phys. Rev. D* **2007**, *76*, 103533, doi:10.1103/PhysRevD.76.103533.
56. Li, H.; Xia, J.Q.; Zhao, G.B.; Fan, Z.H.; Zhang, X. On Using the WMAP Distance Information in Constraining the Time-evolving Equation of State of Dark Energy. *ApJ* **2008**, *683*, L1, doi:10.1086/591082.
57. Eisenstein, D.J.; Hu, W. Baryonic Features in the Matter Transfer Function. *ApJ* **1998**, *496*, 605–614, doi:10.1086/305424.
58. Fialkov, A.; Loeb, A. Constraining the CMB optical depth through the dispersion measure of cosmological radio transients. *J. Cosmol. Astropart. Phys.* **2016**, *2016*, 004, doi:10.1088/1475-7516/2016/05/004.